Oxygen Adsorption on CdSe Surfaces: Case Study of Asymmetric Anisotropic Growth through ab Initio Computations

G. Pilania, T. Sadowski, and R. Ramprasad*

Chemical, Materials, and Biomolecular Engineering, Institute of Materials Science, University of Connecticut, Storrs, Connecticut 06269

Received: August 21, 2008; Revised Manuscript Received: October 30, 2008

Asymmetric anisotropic growth in wurtzite based II−VI semiconductors has been exploited in the past to create a diversity of nanocrystal shapes and topologies. Here, we present a methodology, based on ab initio calculations, to assess the circumstances (i.e., chemical environments) under which anisotropic and asymmetric growth could occur in terms of the ordering and magnitude of the surface energies. This methodology is applied to wurtzite CdSe systems exposed to oxygen atmospheres. Our results show that oxygen adsorption, in the most favored binding mode, is exothermic on all polar and nonpolar CdSe facets. On nonpolar facets, which contain equal numbers of Cd and Se atoms, adsorption of oxygen takes place preferentially on Se resulting in very stable surface configurations with large drops in surface energy (relative to the clean surfaces). This renders all nonpolar facets passive toward growth in the presence of oxygen. Among the four major inequivalent polar surface facets, two (the Cd-terminated and Se-terminated (0001) surfaces) can be successively created on one side of the nanocrystal and two other facets (the Cd-terminated and Se-terminated (000$\bar{1}$) surfaces) can be successively created only on the opposite side. For growth to occur along either the (0001) or the (000$\bar{1}$) directions, *both* (0001) surfaces or *both* (000$\bar{1}$) surfaces, respectively, should display high surface energies relative to all other surfaces. We find that, for appropriate choices of the Cd chemical potential and oxygen coverage, the surface energies of the two (0001) facets are far higher than any of the other surfaces, thereby making (0001) facets relatively unstable and prone to rapid growth along only that direction (resulting in asymmetric anisotropic growth). Thus by controlling the ordering of the surface energies (e.g., through proper choices of precursor concentration and surfactants), control of directional growth can be achieved, as has been done before empirically.

I. Introduction

In recent years, colloidal chemistry methods have resulted in unprecedented control of the sizes and shapes of semiconductor nanostructures,[1−3] which translates to control of a wide range of electrical, electronic, and optical properties. These efforts have been motivated by numerous important applications in diverse technological fields that include photovoltaic cells,[4,5] displays,[6] biological tags,[7,8] and lasers.[9] Nanocrystals grown in solution are usually prepared in the presence of surfactants which are continuously adsorbed and desorbed from the surface allowing the nanocrystal to grow in a controlled manner. While the growth of a nanocrystal is governed by factors related to both thermodynamics (e.g., surface energies) and kinetics (e.g., activation energies for adsorption/desorption), the equilibrium shape of the crystal under a given set of processing conditions is largely determined by the thermodynamics. This philosophy has been at the heart of approaches related to the Wulff construction.[10] Thus, an intricate knowledge of the surface energies for a wide variety of surfaces in the presence of various surfactant molecules could provide guidance for synthetic colloidal chemistry. Such efforts are already underway, and have been used as part of both experimental[11,12] and computational[13−15] studies to understand the properties of several semiconductor nanocrystals in the presence of model adsorbates.

An interesting and potentially useful phenomenon observed in wurtzite semiconductor nanocrystals is asymmetric anisotropic
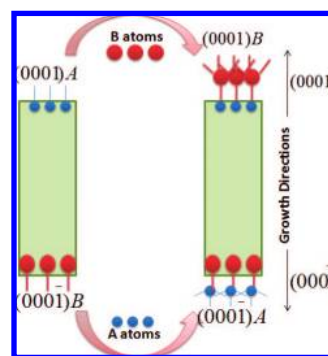
Figure 1. Schematic diagram showing the evolution of polar facets during asymmetric growth in a rod-shaped AB wurtzite crystal. Note that out of four distinct polar facets two can only occur on the top and the other two can only occur on the bottom surface of the growing crystal.

growth. While anisotropic growth in wurtzite systems refers to preferred growth along one dimension (say, the *c*-axis) over others, *asymmetric* anisotropic growth refers to a strong preference to grow along only one of the two complementary anisotropic axes (say, along the positive *c*-axis rather than along the negative *c*-axis). The inherent asymmetry between the positive and negative *c*-axes for a compound wurtzite semiconductor (made from A and B atoms) is schematically illustrated in Figure 1. It can be seen that while the A-terminated and B-terminated (0001) facets have one and three dangling bonds, respectively, the A-terminated and B-terminated (000$\bar{1}$)

* Corresponding author. E-mail: rampi@ims.uconn.edu.

facets have three and one dangling bonds, respectively. Thus, these systems display four *inequivalent* {0001} surface facets, with two of them occurring exclusively on one side and the other two on the opposite side. Therefore, growth along one direction will be controlled by one pair of surfaces, while growth along the opposite direction will be controlled by a different pair of surfaces. Since different conditions can stabilize the surfaces to different extents (and hence growth rates), asymmetric growth has become possible, and has been exploited (through control of surfactants, ambient atmospheres, and temperature) in the creation of a wide diversity of structures, including nanorods, nanoribbons/nanobelts, nanosaws, nanoflowers, and tetrapods starting from spherical CdSe, CdTe, ZnO, ZnS, and CdS colloidal nanocrystals.[1,16−24]

In the present paper, we focus on wurtzite CdSe as a model system, as this is one of the most important, frequently studied, and versatile II−VI compound semiconductors. Not only has asymmetric growth been demonstrated in this system through control of temperature, ambient conditions, and precursor concentration,[24−27] but it has also been observed that exposure to oxygen at low temperatures leads to the formation of asymmetric CdSe nanorods from originally spherical nanocrystals (with minimal change in the diameter).[28] While ab initio computations have been performed in the past to understand the reasons for anisotropic growth of CdSe nanocrystals,[11,12,29,30] mechanisms underlying *asymmetric* growth have not been studied in detail. It appears that a fundamental study of the factors controlling the asymmetric growth of wurtzite nanostructures would help further extend our understanding of shape control of nanostructures.

The present study starts with a comprehensive reassessment of the various surface energies of wurtzite CdSe, and the changes in these surface energies as a function of oxygen coverage. Surfaces of wurtzite CdSe explored in the present study are the nonpolar $(10\bar{1}0)$, $(01\bar{1}0)$, and $(11\bar{2}0)$ facets and the polar Cd-terminated (0001), Se-terminated (0001), Cd-terminated $(000\bar{1})$, and Se-terminated $(000\bar{1})$ facets. The nonpolar facets display low surface energies in the presence or absence of oxygen, and are expected to be passive to growth. The polar facets, on the other hand, owing to their larger surface energies, control the degree of anisotropic growth. In addition, we will point out that the drastically different ordering and magnitude of the nonpolar surface energies (and their dependence on the presence or absence of oxygen, and precursor and surfactant concentrations) are expected to play a crucial role in controlling asymmetric anisotropic growth. Moreover, we will find that asymmetric growth is more a rule than an exception in these (and perhaps other) wurtzite systems, owing to the vastly different surface energies of the (0001) and $(000\bar{1})$ based facets. The choice of oxygen as an adsorbate has an added advantage. It has allowed us to probe the nature of the various surface facets considered, in terms of surface unsaturations, dangling bonds, and valence electron counts.

The remainder of the paper is organized as follows. In section II, we describe technical aspects pertaining to our first principles calculations and CdSe surface models. Details concerning the determination of surface energies in the presence and absence of O adsorbates are discussed in section III. Our results are presented in section IV, followed by a discussion of the implications of our results for asymmetric growth in section V. Finally, we collect our conclusions in section VI.
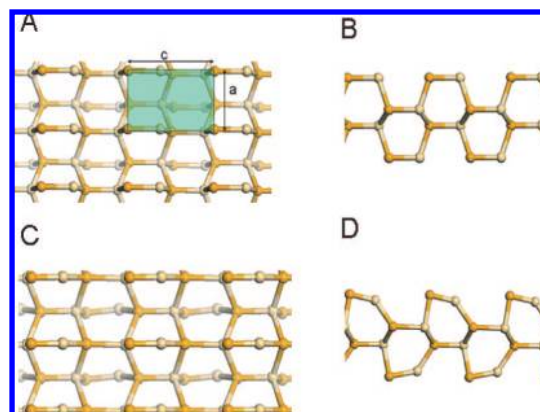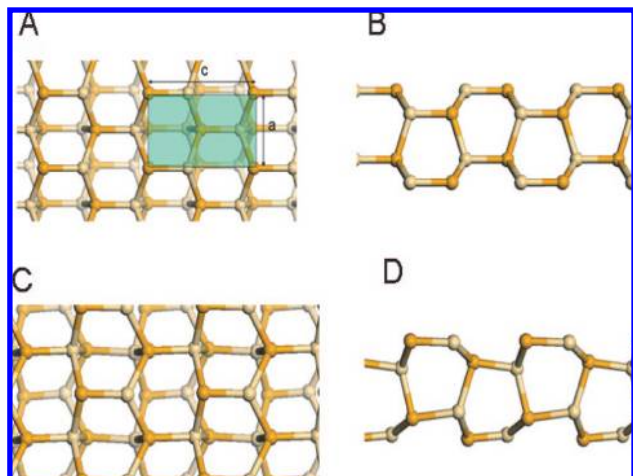

Figure 2. Top and side views of the nonpolar $(01\bar{1}0)$ facet before (A, B) and after (C, D) relaxation. Se atoms are colored yellow, and Cd atoms are colored gray. The primitive surface unit cell is highlighted in panel A.

II. Methods

II.A. Computational Details. All results presented here were performed using density functional theory (DFT) at the local density approximation (LDA) as implemented within SIESTA,[31] a local orbital DFT code.[32] Cd and Se core electrons were described by norm-conserving nonlocal pseudopotentials of the Troullier−Martins type[33] with atomic configurations of [Kr]$4d^{10}5s^25p^0$ and [Ar $3d^{10}$]$4s^24p^4$, respectively. A double-ζ plus polarization (DZP) basis set was used for all calculations with an orbital confining cutoff radius specified by an energy shift parameter of 0.006 Ry. A Monkhorst−Pack k-point mesh of $6 \times 6 \times 4$ yielded well converged bulk results. As a test of pseudopotentials and computational method, bulk wurtzite CdSe calculations were performed. The calculated a and c lattice constants were 4.29 Å and 6.82 Å, in good agreement with prior work at the same level of theory,[34,35] and with the corresponding experimental values.[36] Surface calculations employed a Monkhorst−Pack k-point mesh of $6 \times 6 \times 2$ to yield converged results. Relaxation of the surface structures was accomplished by requiring the forces experienced by each atom to be smaller than 0.04 eV/Å.

II.B. Description of the Surface Facets. Surfaces of wurtzite CdSe may be polar or nonpolar, depending on the stoichiometry of the atoms contained in the surface plane. Nonpolar surfaces are stoichiometric, containing equal numbers of Cd and Se atoms. In the present work, we have considered the three most stable nonpolar facets, viz., $(10\bar{1}0)$, $(01\bar{1}0)$, and $(11\bar{2}0)$. Schematics of the starting geometry of slabs containing these surfaces are shown in Figures 2, 3, and 4 (panels A and B). The corresponding relaxed geometries, shown in Figures 2−4 (panels C and D), will be discussed in section IV. We note that while each surface atom on the $(01\bar{1}0)$ surface displays two dangling bonds, those on the $(10\bar{1}0)$ and $(11\bar{2}0)$ surfaces display one dangling bond. This observation will be relevant in the discussion of surface relaxation and energetics. The primitive surface unit cells for the $(01\bar{1}0)$ and $(10\bar{1}0)$ facets highlighted in Figures 2A and 3A, respectively, contain one surface Cd atom and one surface Se atom. Owing to the lower symmetry of the $(11\bar{2}0)$ facet, its primitive surface unit cell contains two Cd and two Se atoms (shown in Figure 4A).

In addition to the three nonpolar facets, the following four polar facets were also considered: Cd-terminated and Se-terminated (0001) surfaces (referred to henceforth as (0001)Cd and (0001)Se, respectively) and the Cd-terminated and Se-terminated $(000\bar{1})$ surfaces (referred to as $(000\bar{1})$Cd and

Oxygen Adsorption on CdSe Surfaces

J. Phys. Chem. C, Vol. 113, No. 5, 2009 **1865**

Figure 3. Top and side views of the nonpolar $(10\bar{1}0)$ facet before (A, B) and after (C, D) relaxation. Se atoms are yellow, and Cd atoms are gray. The primitive surface unit cell is highlighted in panel A.
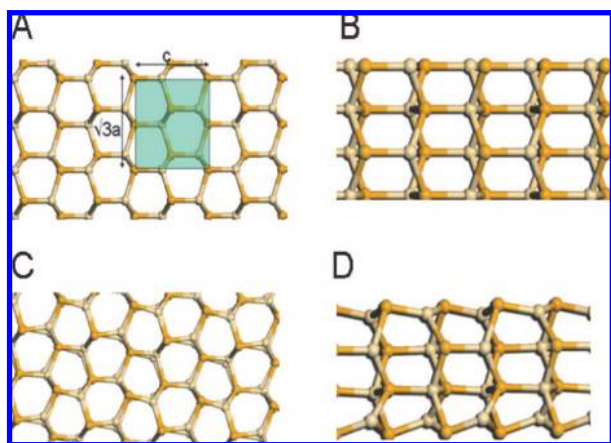
Figure 4. Top and side views of the nonpolar $(11\bar{2}0)$ facet before (A, B) and after (C, D) relaxation. The primitive surface unit cell is highlighted in panel A.
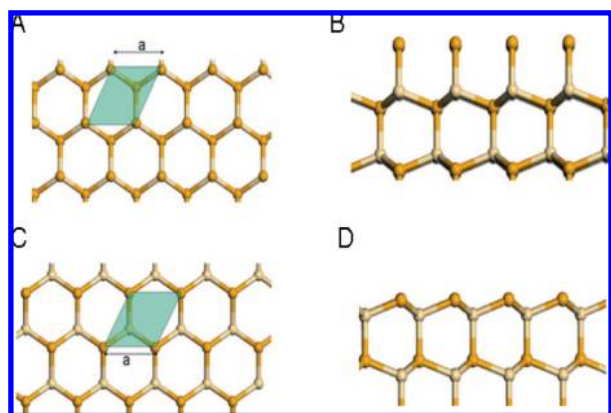
Figure 5. Top and side view of the relaxed polar (0001)Se (A, B) and $(000\bar{1})$Se (C, D) facets. The primitive surface unit cell is highlighted in each case. The complementary Cd-terminated surfaces are obtained by interchanging the yellow and gray atoms.

$(000\bar{1})$Se, respectively). The (0001)Cd facet and its complementary $(000\bar{1})$Se facet have one dangling bond per surface atom, while the $(000\bar{1})$Cd facet and its complementary (0001)Se facet have three dangling bonds per surface atom, as shown schematically in Figure 5. Each surface atom can be associated with a primitive cell, as highlighted in Figure 5A,C.

All slabs considered in the present work, each containing a top and a bottom surface, were two bulk lattice units thick in the direction normal to the surface. A vacuum of approximately 12 Å was placed above the slabs in order to avoid any spurious interaction between adjacent slabs along the slab surface normals.

III. Thermodynamic Details

III.A. Relaxed Surface Energies. In the case of nonpolar surfaces having identical terminations on the top and bottom surfaces of the slab, the surface energy (after all the atoms have been allowed to relax to their equilibrium positions) is given by

$$\sigma_{\text{relaxed}}^{\text{np}} = \frac{E_{\text{slab,relaxed}} - n_{\text{CdSe}} E_{\text{bulk,CdSe}}}{2A} \quad (1)$$

where $E_{\text{slab,relaxed}}$ is the total energy of the geometry-optimized (or "relaxed") slab, n_{CdSe} is the number of CdSe pairs in the slab, $E_{\text{bulk,CdSe}}$ is the total energy per CdSe pair of bulk wurtzite CdSe, and A is the surface area. The factor 2 accounts for the presence of two identical (top and bottom) surfaces, and the superscript "np" represents nonpolar surfaces.

In the case of polar surfaces, if we require that our slab system contains an integer number of CdSe pairs (so that a bulk reference energy is available to determine surface energies), the top and bottom surfaces will be inequivalent (e.g., (0001)Cd and $(000\bar{1})$Se, or (0001)Se and $(000\bar{1})$Cd). On the other hand, if we make both the top and bottom surfaces Cd-terminated (or both Se-terminated), we will lose the ability to define a suitable bulk reference (as in this case we will not have an integer number of CdSe pairs). Furthermore, in the case of wurtzite CdSe, the latter possibility will still lead to inequivalent top and bottom surfaces (e.g., (0001)Cd and $(000\bar{1})$Cd, or (0001)Se and $(000\bar{1})$Se) due to the lack of inversion symmetry.

Owing to these complications, it is necessary to introduce the chemical potential of either Cd or Se, as well as to go beyond slab supercell methods to determine the surface energy of polar surfaces, as has been elaborately discussed elsewhere.[29,37]

In the present work, we used the chemical potential of Cd (μ_{Cd}), which as described by others,[14,29] has to satisfy the following bounds:

$$E_{\text{bulk,Cd}} + \Delta H_{\text{f,CdSe}} \le \mu_{\text{Cd}} \le E_{\text{bulk,Cd}} \quad (2)$$

where $\Delta H_{\text{f, CdSe}}$ is the heat of formation of CdSe from elemental Cd and Se, and $E_{\text{bulk,Cd}}$ and $E_{\text{bulk,Se}}$ are the energy per Cd and Se atom, respectively, of the corresponding elemental bulk systems obtained from separate total energy calculations. We will define the two extreme values for μ_{Cd} as those related to a Cd atom in a Cd-poor (minimum μ_{Cd}) CdSe crystal and in a Cd-rich (maximum μ_{Cd}) CdSe crystal. Surface energies are linearly related to μ_{Cd} over this allowed range.[14] We note that, although the allowed range of μ_{Cd} can be properly defined, identification of the value of μ_{Cd} corresponding to specific chemical conditions is nontrivial. For instance, the Gibbs–Thompson equation implies that the chemical potential will vary with the size of a nanocrystal.[38] Here, we use μ_{Cd} as a semiquantitative measure of the chemical environment (i.e., the Cd precursor concentration) in which the nanocrystal is growing.

Furthermore, in the present work, rather than go beyond the slab supercell treatment, we have used the (0001)Cd surface energy values under Cd-rich and Cd-poor conditions as calculated by Manna et al., combined with three separate slab geometry calculations involving polar surfaces to determine all

μ_{Cd}-dependent polar surface energies, as described below. These energies form the baseline for our investigation of the impact of oxygen adsorption on CdSe surfaces.

Slab 1 had (0001)Cd and (000$\bar{1}$)Se facets as the top and bottom surfaces. The sum of the surface energies of the top and bottom surfaces of slab 1 is given as

$$\sigma_{\text{relaxed}}^{(0001)\text{Cd}} + \sigma_{\text{relaxed}}^{(000\bar{1})\text{Se}} = \frac{E_{\text{slab1,relaxed}} - n_{\text{CdSe}}E_{\text{bulk,CdSe}}}{A} \quad (3)$$

Manna et al.[14] report a (0001)Cd surface energy value of 95 meV/Å^2 under Cd-poor conditions (i.e., when $\mu_{Cd} = E_{\text{bulk, Cd}} + \Delta H_{\text{f, CdSe}}$) and 75 meV/Å^2 under Cd-rich conditions (i.e., when $\mu_{Cd} = E_{\text{bulk, Cd}}$). Using these values, we have computed the surface energies of the (000$\bar{1}$)Se surface across the allowed range of μ_{Cd} by noting that $\sigma_{\text{relaxed}}^{(0001)\text{Cd}}$ and $\sigma_{\text{relaxed}}^{(000\bar{1})\text{Se}}$ are linearly dependent on μ_{Cd} (although their sum is a constant).

Our second slab (slab 2) contained the (0001)Cd and (000$\bar{1}$)Cd facets as the top and bottom surfaces. Since these two facets are not complementary facets, the slab does not have an integer number of CdSe pairs. Thus the sum of the surface energies of the top and bottom surfaces will explicitly depend on μ_{Cd}, and is given by

$$\sigma_{\text{relaxed}}^{(0001)\text{Cd}} + \sigma_{\text{relaxed}}^{(000\bar{1})\text{Cd}} = \frac{E_{\text{slab2,relaxed}} - n_{\text{Cd}}\mu_{\text{Cd}} - n_{\text{Se}}\mu_{\text{Se}}}{A} =$$

$$\frac{E_{\text{slab2,relaxed}} - (n_{\text{Cd}} - n_{\text{Se}})\mu_{\text{Cd}} - n_{\text{Se}}E_{\text{bulk,CdSe}}}{A} \quad (4)$$

where n_{Cd} and n_{Se} are the number of Cd and Se atoms in the slab, respectively. Since the μ_{Cd}-dependent surface energy of the (0001)Cd facet is available from ref 14, the μ_{Cd}-dependent (000$\bar{1}$)Cd surface energy was obtained from eq 4.

Finally, the μ_{Cd}-dependent (0001)Se surface energy was computed using slab 3, which had the (000$\bar{1}$)Cd and (0001)Se complementary facets as the top and bottom surfaces, using a procedure analogous to the one adopted in the case of slab 1 and using the μ_{Cd}-dependent surface energy values for (000$\bar{1}$)Cd obtained from the slab 2 calculation. Thus, all the polar surface energies across the range of allowed chemical potentials were determined using the literature value for one surface energy at the two extreme values of the Cd chemical potential.

III.B. Surface Relaxation Energies. In the present work, we define the surface relaxation energy per unit area to be the difference between surface energies of the bulk terminated unrelaxed and relaxed surfaces. Thus, the relaxation energy for a nonpolar surface can be calculated from the difference in total energies of the unrelaxed slab $E_{\text{slab,unrelaxed}}$ and of the same slab after full relaxation using

$$\Delta\sigma_{\text{relaxation}}^{\text{np}} = \frac{E_{\text{slab,unrelaxed}}^{\text{np}} - E_{\text{slab,relaxed}}^{\text{np}}}{2A} \quad (5)$$

In the case of a slab containing different top and bottom polar surface terminations, the surface relaxation energy of each terminating polar facet was determined by fixing the top or bottom half of the slab atoms at their bulk positions and letting the remaining atoms relax to their equilibrium positions. The surface relaxation energy is given by

$$\Delta\sigma_{\text{relaxation}}^{\text{p}} = \frac{E_{\text{slab,unrelaxed}}^{\text{p}} - E_{\text{slab,relaxed}}^{\text{p}}}{A} \quad (6)$$

where the superscript "p" represents polar surfaces.

III.C. O-Covered Surfaces. In this study, we considered the binding of O atoms to the nonpolar and polar surfaces described

TABLE 1: Surface Relaxation Energy (in meV/Å^2) of Various CdSe Wurtzite Facets

facet	$\Delta\sigma_{\text{relaxation}}$
(10$\bar{1}$0)	21.20
(01$\bar{1}$0)	45.12
(11$\bar{2}$0)	34.83
(0001)Cd	10.23
(000$\bar{1}$)Se	11.20
(000$\bar{1}$)Cd	12.71
(0001)Se	11.90

above. O coverages ranging from zero to one monolayer have been studied. In order to quantify the impact of O passivation, we focus on the O binding energy and the surface energy of the O-covered surface, as a function of O coverage. We define the binding energy (E_b) due to the adsorption of an O atom (for a given surface coverage) as the energy released per adsorbed O atom, given as

$$E_{\text{b}} = \frac{E_{\text{slab,relaxed}} + \frac{n_{\text{O}}}{2}\mu_{\text{O}_2,\text{gas}} - E_{\text{slab,relaxed,O}}}{n_{\text{O}}} \quad (7)$$

where n_{O} is the number of O atoms adsorbed on the surface, $\mu_{\text{O}_2,\text{gas}}$ is the chemical potential of O_2 in the gas phase (taken here to be the DFT total energy of an O_2 molecule), and $E_{\text{slab,relaxed,O}}$ is the total energy of the slab with O atoms on one side of the slab on the surface of interest. The surface energy of the O-covered surface was calculated using

$$\sigma_{\text{relaxed,O}} = \sigma_{\text{relaxed}} - n_{\text{O}}E_{\text{b}}/A \quad (8)$$

Finally, we mention that adsorption of O on surfaces is a multistep process, involving physisorption of O_2, followed by O–O bond breakage, and finally chemisorption of atomic O, with activation barriers associated with the adsorption process. As we are primarily concerned with the thermodynamics of adsorption in this paper, we do not consider these initial steps. Also, finite temperature effects[39] have not been taken into account in the present study. While this factor may be important in general, the qualitative aspects of our main conclusions, which rely on the ordering and *relative* magnitudes of surface energies, are not expected to change considerably.

IV. Results

IV.A. Surface Relaxation. Our results for the optimized slab geometries are in good agreement with prior work[14,15,40] and, in general, conform to the electron counting rules for II–VI semiconductor systems proposed earlier.[41] Since Cd and Se have nominal valences of 2 and 6, respectively, sp^3 hybridization in bulk CdSe requires that a Cd atom contributes 1/2 electron to each of its four bonds to Se, and an Se atom contributes 3/2 electrons to each of its four bonds to Cd. Atoms at a surface display lower coordination, and hence unshared electrons. By suitable relaxation and reconstruction, a surface attempts to minimize its energy by optimally sharing the electrons at the surface, i.e., by rehybridizing, and the extent to which this is accomplished will depend on the nature of the surface and the number of unshared electrons.

In the case of the nonpolar (01$\bar{1}$0), (10$\bar{1}$0), and (11$\bar{2}$0) surfaces significant relaxation was observed, accompanied by significant surface relaxation energies as listed in Table 1. In general, comparison of initial and relaxed structures shows that surface Cd atoms move inward toward the bulk and the surface Se atoms tend to move outward, resulting in a tilting of the surface CdSe bond relative to the horizontal (see, for instance, panels B and
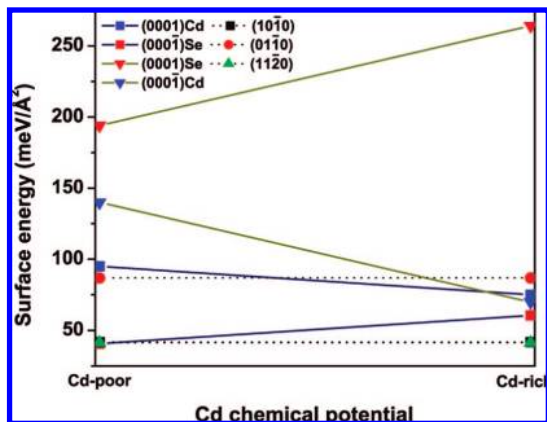
Oxygen Adsorption on CdSe Surfaces

J. Phys. Chem. C, Vol. 113, No. 5, 2009 **1867**

Figure 6. Surface energies for unpassivated polar and nonpolar facets as a function of Cd chemical potential.

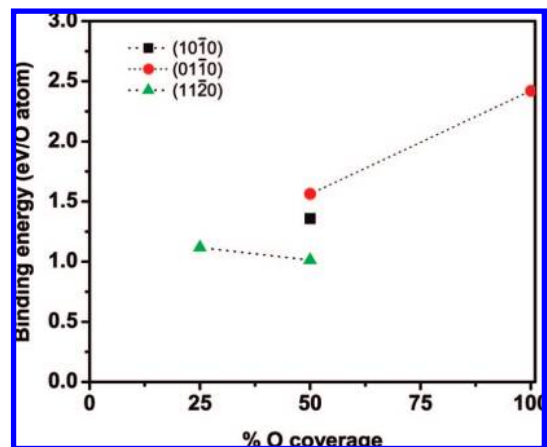**Figure 8.** Surface energies of nonpolar CdSe facets as a function of oxygen passivation.

Figure 7. Energy released per adsorbed oxygen atom on nonpolar CdSe facets, as a function of surface passivation.

Figure 9. Top and side views of 3-fold, bridge, and on-top (A, B, C) adsorption sites for oxygen on polar facets.

D of Figures 2−4). This relaxation behavior can be understood in terms of the transfer of electrons from the Cd atoms to the more electronegative Se atoms at the surface. We note that, in the case of the $(01\bar{1}0)$ surface, each surface atom displays two dangling bonds, while the $(10\bar{1}0)$ and $(11\bar{2}0)$ surface atoms display one dangling bond each. Thus, Cd atoms at $(10\bar{1}0)$ and $(11\bar{2}0)$ surfaces can donate their unshared 1/2 electron to the surface Se atoms, resulting in a more planar 3-fold configuration around the surface Cd atom accompanied by the inward movement of surface Cd atoms, as seen before in CdSe quantum dots[35] and quantum wires.[34] The surface Se atoms, on the other hand, possess a doubly filled dangling bond, which is preferentially exposed to any incoming electronegative species (such as O as discussed below). A similar, but more intensified, process occurs at the $(01\bar{1}0)$ surface as the surface atoms contain two dangling bonds to begin with. Thus, the $(01\bar{1}0)$ surface relaxation is more pronounced.

In the case of the polar (0001)Cd, $(000\bar{1})$Cd, (0001)Se, and $(000\bar{1})$Se surfaces, no significant relaxation was observed. As these surfaces have only one type of atomic species (either Cd or Se, with one or three dangling bonds), transfer of electrons from the dangling bonds is not possible (at least for the surface unit cells considered here) and hence there is no clear pathway available for relaxation. Thus, the surface relaxation energies of nonpolar facets were found to be significantly smaller than those of nonpolar facets (Table 1).

IV.B. Unpassivated Surface Energies. The surface energies of all relaxed surfaces were computed using the procedure described in section III.A, and are shown in Figure 6 over the
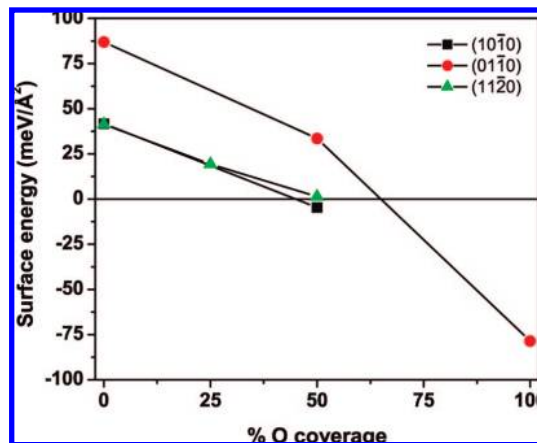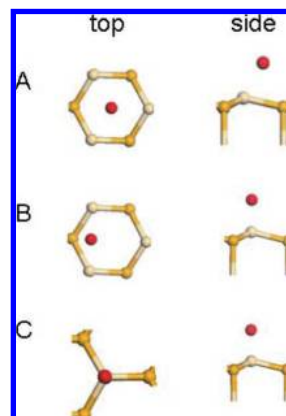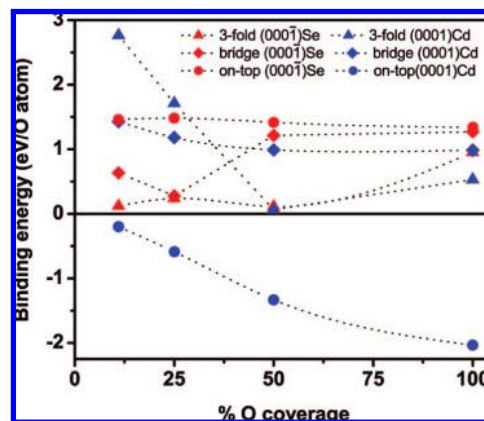

Figure 10. Binding energy of oxygen atom on polar (0001)Cd and $(000\bar{1})$Se facets, as a function of surface passivation for different oxygen adsorption sites.

allowed range of μ_{Cd} values. The surface energies of nonpolar surfaces do not depend on μ_{Cd} and therefore are shown as horizontal lines in the plot. Interestingly, the two nonpolar surfaces with one dangling bond per surface atom, $(10\bar{1}0)$ and $(11\bar{2}0)$, were found to have the same surface energy (41 meV/Å^2). These results are in close agreement with those reported by Manna et al.[14] (42 and 37 meV/Å^2, respectively, for the $(10\bar{1}0)$ and $(11\bar{2}0)$ facets). The surface energy for the $(01\bar{1}0)$ facet was calculated to be 87 meV/Å^2. Its higher value relative to the $(10\bar{1}0)$ and $(11\bar{2}0)$ surfaces is justified by the larger number of dangling bonds per surface atom on this surface.

TABLE 2: Bond Lengths and Binding Energies of Oxygen on CdSe Polar Facets

surface	site	binding energy (eV/atom)				bond length (Å)	
		oxygen coverage				Cd−O	Se−O
		11%	25%	50%	100%		
(0001)Cd	3-fold	2.76	1.71	0.06	0.53	2.35	
	bridge	1.43	1.18	1.00	0.98	2.22	
	on-top	−0.20	−0.59	−1.33	−2.03	2.03	
(000$\bar{1}$)Se	3-fold	0.12	0.23	0.11	0.95		1.72
	bridge	0.63	0.28	1.21	1.27		1.67
	on-top	1.46	1.48	1.41	1.34		1.54
(000$\bar{1}$)Cd	3-fold		2.68	2.96	1.73	2.49	
	bridge		2.34	2.15	1.61	2.19	
	on-top		0.05	−0.18	−0.53	1.94	
(0001)Se	3-fold		8.18	4.96	2.83		1.60
	bridge		9.18	5.45	2.89		1.60
	on-top		9.85	6.08	2.37		1.56

Turning to polar facets, it is apparent from Figure 6 that the sums of surface energies for the two pairs of complementary polar facets, $\sigma[(0001)Cd] + \sigma[(000\bar{1})Se]$ and $\sigma[(000\bar{1})Cd] + \sigma[(0001)Se]$, are always constant and are equal to 68 and 167 meV/Å^2, respectively. The stability of the Cd-terminated polar surfaces increases as we move from Cd-poor to Cd-rich conditions, while the Se-terminated polar surfaces display the opposite behavior. Comparison between the polar surfaces with three dangling bonds per surface atom reveals that (000$\bar{1}$)Cd surface is more stable than (0001)Se surface throughout the range of chemical potential considered. On the other hand, in the case of polar surfaces with one dangling bond per surface atom, the (000$\bar{1}$)Se surface is more stable than the (0001)Cd surface for the entire range of allowed μ_{Cd}.

IV.C. Oxygen Adsorption on Nonpolar Facets. On nonpolar surfaces, it was found that oxygen has a strong tendency to adsorb on Se surface atoms and stable configurations were achieved when each Se dangling bond was passivated by an O atom (i.e., when O atoms were placed at locations close to the missing neighbors of the surface Se atoms). Coordination of O atoms to surface Cd atoms did not result in stable configurations. These observations are entirely consistent with the charge transfer notions discussed in section IV.A, that electron transfer from Cd to Se atoms at the surface results in surface Se atoms with one dangling bond in the case of (10$\bar{1}$0) and (11$\bar{2}$0) surfaces and two dangling bonds in the case of (01$\bar{1}$0) surfaces. Each dangling bond contains two electrons available for donation or bonding with an O atom. Thus, in the case of the (10$\bar{1}$0) surface, which contains one Se atom and one Cd atom per surface unit cell (and one "rehybridized" dangling bond per Se atom), the maximum possible stable O coverage was one O atom per surface unit cell (50% surface coverage). The (11$\bar{2}$0) surface contains two CdSe pairs per surface unit cell, and hence, a 25% surface O coverage representing one O atom per surface unit cell bound to one of the two surface Se atoms and a 50% O coverage corresponding to an O atom bound to each of the two surface Se atoms were possible. Finally, in the case of the (01$\bar{1}$0) surface which contains a CdSe pair per unit cell but with Se atom displaying two dangling bonds, 50% (one O atom per surface Se atom) and 100% (two O atoms per surface Se atom) surface O coverages were possible, and investigated.

Figure 7 shows the binding energy per O atom for all nonpolar surfaces and surface O coverages considered. It can be seen that the binding of O atoms in all these cases is exothermic. The binding energy per O atom on the (11$\bar{2}$0) facet is 1.1 eV for both 25% and 50% surface O coverage, while that for the (10$\bar{1}$0) surface is a little higher (1.4 eV) for 50% passivation. In contrast to the (11$\bar{2}$0) facet, the binding energy on the (01$\bar{1}$0)

facet is a function of surface coverage. This result can be explained by considering that, unlike on the (11$\bar{2}$0) facet, two O atoms are adsorbed on the same Se atom on the (01$\bar{1}$0) surface. The adsorption of the second oxygen atom on the same Se atom is even more exothermic compared to the first one.

Figure 8 displays the surface energies of the considered oxygen passivated nonpolar facets as a function of surface coverage. Owing to the exothermic nature of O adsorption on all the nonpolar facets considered, the oxygen passivated nonpolar facets have significantly lower surface energies compared to unpassivated relaxed facets. Owing to the constant binding energy, the surface energy of the (11$\bar{2}$0) surface decreases at a constant rate as we increase oxygen passivation from 0 to 50%. However, the surface energy of (01$\bar{1}$0) facet decreases at an increasing rate on oxygen passivation due to the increasing exothermicity of the adsorption process. These results show that when exposed to an appropriate level of oxygen atmosphere, nonpolar facets will tend to adsorb oxygen and attain a thermodynamically stable configuration, hindering further growth of these facets.

IV.D. Oxygen Adsorption on Polar Facets. The polar CdSe surfaces revealed a much richer variety of O binding modes than the nonpolar surfaces. Three different adsorption sites, namely, 1-fold (or on-top), 2-fold (or bridge), and 3-fold, were considered. These binding modes are shown in Figure 9. In each case, O was initially placed 2 Å above the surface. Again, as in nonpolar facets, we define 100% surface passivation as the configuration corresponding to one O atom adsorbed per surface atom. In order to obtain a deeper understanding of the nature of the polar surfaces, and the character of dangling bonds at surface atoms, a large number of surface O coverages (than in the case of nonpolar surfaces) were considered by using 2 × 2 and 3 × 3 surface unit cells.

IV.D.1. Adsorption on (0001)Cd and (000$\bar{1}$)Se Facets (Displaying One Dangling Bond per Surface Atom). Figure 10 and Table 2 report the calculated binding energies for the (0001)Cd and (000$\bar{1}$)Se facets upon passivation with oxygen on the three different adsorption sites. Passivation of 25%, 50%, and 100% represent one, two, and four O atoms adsorbed on a 2 × 2 supercell, respectively. A 3 × 3 cell with one oxygen adsorbed on it was also considered in both (0001)Cd and (000$\bar{1}$)Se cases to calculate the binding energy at a lower surface passivation level of 11%. We find that at low passivation (25% or less) O adsorption at the 3-fold site on (0001)Cd is very stable with high binding energy (2.7 eV), while at higher levels of oxygen passivation the bridge site becomes the most exothermic adsorption site with an almost constant binding energy of 1 eV. We note that the on-top adsorption site on (0001)Cd is the only

Oxygen Adsorption on CdSe Surfaces

J. Phys. Chem. C, Vol. 113, No. 5, 2009 **1869**
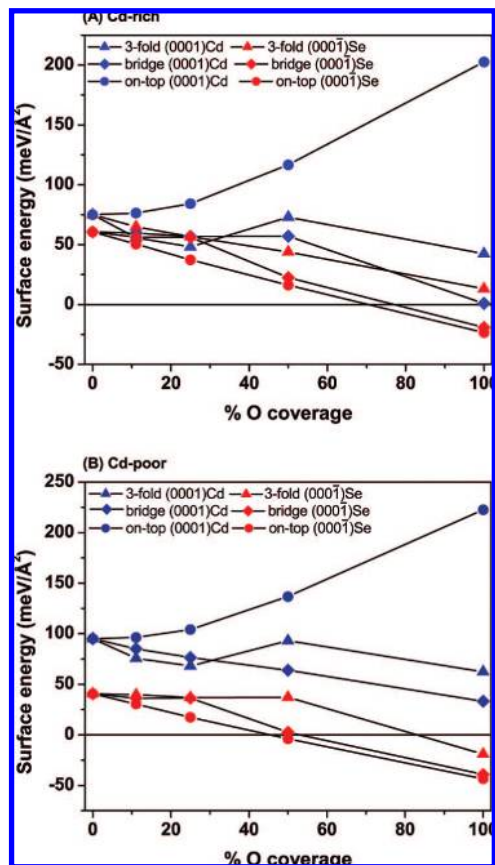
Figure 11. Surface energies of oxygen-passivated (0001)Cd and (000$\bar{1}$)Se facets, as a function of surface passivation. (A) Cd-rich case; (B) Cd-poor case.

Figure 12. Binding energy of oxygen atom on polar (0001)Se and (000$\bar{1}$)Cd facets as a function of surface passivation for different adsorption sites.

endothermic site among all sites considered, with the degree of endothermicity increasing with coverage. For the (000$\bar{1}$)Se facet, energy released is highest when O atoms are adsorbed on the electron-rich on-top site. Calculated Cd–O and Se–O bond lengths for 100% O passivation are also shown in Table 2. We note that the shortest bond length was always achieved for on-top site adsorption while 3-fold adsorption site always results in the longest bond length.

Using eq 8 and the adsorption energies of O shown in Figure 10, the calculated surface energies of (0001)Cd and (000$\bar{1}$)Se facets for the two extreme values of Cd chemical potential (corresponding to Cd-rich and Cd-poor conditions) were calculated and are shown in Figure 11. It can be seen that, for the entire range of O coverages considered, and for both extremes of μ_{Cd}, the (0001)Cd facet displays higher surface energy than the (000$\bar{1}$)Se facet for the most favored O binding mode.

IV.D.2. Adsorption on (000$\bar{1}$)Cd and (0001)Se Facets (Displaying Three Dangling Bonds per Surface Atom). The results of our binding energy calculation for polar facets with three dangling bonds per surface atom are reported in Figure 12 and Table 2. As a general observation, adsorption energy of O on (0001)Se facet is a decreasing function of surface passivation while it is almost constant for the (000$\bar{1}$)Cd facet. This trend is consistent with the observation that O atoms adsorbed on (0001)Se display a propensity to stay above the surface, resulting in increased electrostatic repulsion with coverage, and consequently a drop in binding energy per adsorbed O. On the other hand, adsorbed O atoms on (000$\bar{1}$)Cd tend to penetrate the surface layer (except in the case of the endothermic on-top site binding mode), thereby resulting in an effective "screening" of an O from its neighbors, and a constant
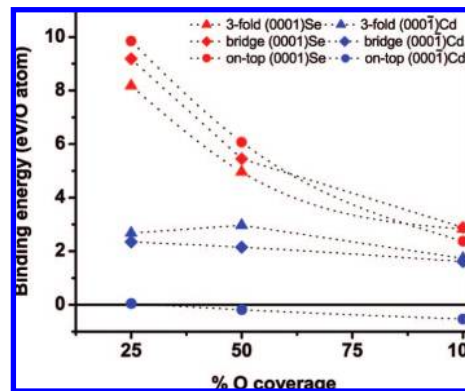
binding energy with increasing coverage. Furthermore, the binding energy of O on the (0001)Se facet was found to be remarkably high at low surface coverages, with the preferred binding mode being the on-top site. As coverage increases, all three binding modes become favored somewhat equally, with the bridge site being slightly preferred over the other two modes. On the (000$\bar{1}$)Cd surface, the 3-fold site is the most preferred across the range of O coverages considered. Consistent with the behavior previously seen in the case of (0001)Cd facet, on-top site O adsorption is endothermic on the (000$\bar{1}$)Cd facet as well.

Figure 13 shows the surface energy of the (0001)Se and (000$\bar{1}$)Cd facets as a function of surface O passivation for two extremes of Cd chemical potential. Features different from those in Figure 11 can be seen. For instance, the ordering of the (0001)Se and (000$\bar{1}$)Cd surface energies depends on the level of O coverage and μ_{Cd}. While the (000$\bar{1}$)Cd surface is more stable than the (0001)Se surface in the absence of O (regardless of μ_{Cd}), the stability trend is reversed when the O coverage exceeds ∼10% under Cd-rich conditions, and is not reversed under Cd-poor conditions. In other words, in an abundant O atmosphere, the relative stability of the (000$\bar{1}$)Cd facet is higher in Cd-poor conditions, while Cd-rich conditions render the (0001)Se facet more stable.

V. Discussion

One of the underlying motivations for the present study was to gain insights into the causes of asymmetric growth in wurtzite semiconductors such as CdSe, as well as to assess the influence of adsorbed oxygen on this type of growth. We make the observation (based on Figure 1) that growth along, say, the (0001) direction occurs through successive and interconvertible creation of (0001)Cd and (0001)Se surfaces. Thus, for vigorous growth to occur preferentially along the (0001) direction, the surface energy of *both* the (0001)Cd and (0001)Se surfaces should necessarily be high relative to that of all other surface facets. Even if one of these two surfaces has a low surface energy, growth along the (0001) direction will be impeded. In fact, this is the situation in the case of clean CdSe surfaces, i.e., in the absence of oxygen adsorbates, as can be inferred from Figure 6 regardless of the value of the Cd chemical potential. Although the (0001)Se surface energy is high, the (0001)Cd surface energy is low (almost as low as that of the stable nonpolar (01$\bar{1}$0) facet). Likewise, growth along the (000$\bar{1}$) direction is also expected to be practically nonexistent in the absence of oxygen as the
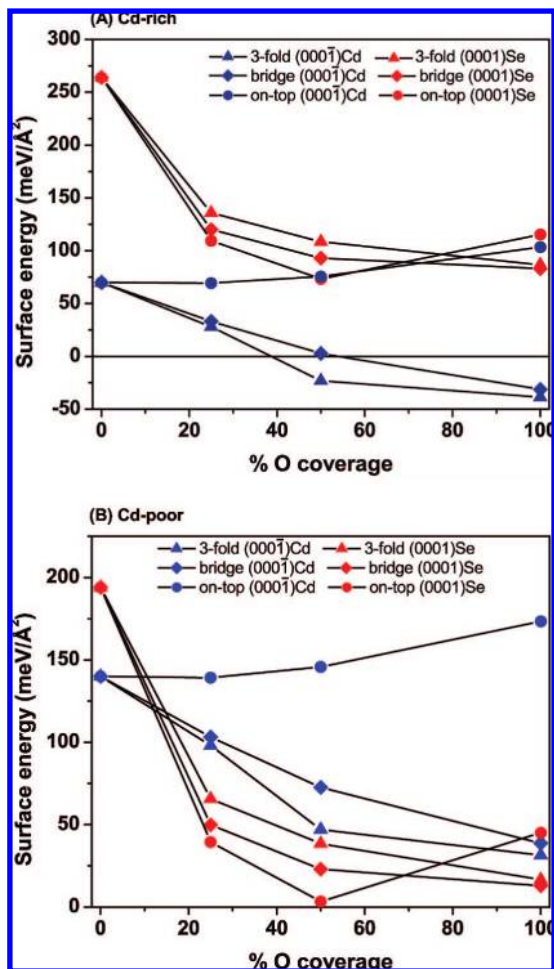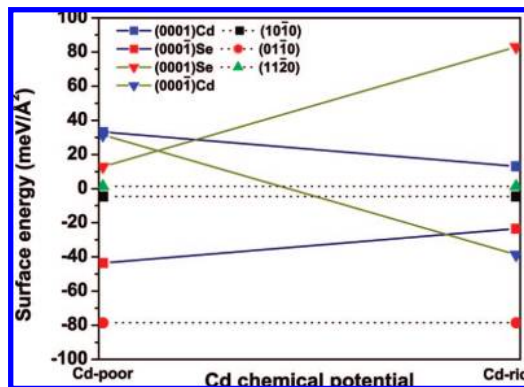
Figure 13. Surface energies of oxygen-passivated (0001)Se and (000$\bar{1}$)Cd facets, as a function of surface passivation. (A) Cd-rich case; (B) Cd-poor case.

Figure 14. Surface energies for oxygen-passivated polar and nonpolar facets as a function of Cd chemical potential. Results corresponding to oxygen adsorption at the most stable adsorption site (most exothermic) and at the maximum possible oxygen coverage are shown.

(000$\bar{1}$)Se surface energy is quite low, for all allowed values of the Cd chemical potential. The only surfaces with large surface energies are the (0001)Se and (000$\bar{1}$)Cd surfaces under Cd-poor conditions, but these are complementary surfaces on opposite sides of the nanocrystal, and so cannot enable active growth along either direction. For these reasons, in the absence of surfactants and conditions that could drastically change the ordering and magnitude of surface energies from the values predicted in Figure 6, CdSe nanocrystals are not expected to display asymmetric *or* anisotropic growth, and will be roughly spherical.

The picture changes dramatically when the surfaces are exposed to oxygen. Based on the results pertaining to oxygen adsorption from the previous section, Figure 14 has been created, which is analogous to Figure 6 that applies to clean surfaces. For clarity, Figure 14 shows the surface energy results corresponding to surfaces with the highest achievable level of oxygen passivation considered here, and for the most stable oxygen binding modes. For instance, results corresponding to 50% oxygen passivation for the (11$\bar{2}$0) facet and 100% oxygen passivation for all the other facets are displayed. Our conclusions that follow from Figure 14 are listed below.

1. We note that the ordering of surface energy for both polar and nonpolar facets changes significantly upon O passivation.

2. In the case of all the nonpolar facets, the propensity for O adsorption far outweighs the energy needed to create the surfaces in the first place, resulting in net negative values for the surface

energy. O adsorption thus renders all these surfaces very stable, and passive to further growth.

3. The O-covered (000$\bar{1}$)Cd surface displays negative surface energy (and, hence, is very stable) under Cd-rich conditions, but displays large values (and is relatively unstable) under Cd-poor conditions. However, the (000$\bar{1}$)Se surface displays a low (negative) surface energy, regardless of the choice of the μ_{Cd} value. This behavior of the (000$\bar{1}$)Se surface (notwithstanding the μ_{Cd} dependence of the (000$\bar{1}$)Cd surface energy) implies a sluggishness of growth along the (000$\bar{1}$) direction, for the entire allowed μ_{Cd} range.

4. *Both* the (0001)Cd and (0001)Se surfaces display large positive values of the surface energy relative to all other surfaces for a large range of allowed intermediate μ_{Cd} values, indicating the possibility of preferential growth along the (0001) direction.

In addition, we note that preferential growth along the (000$\bar{1}$) direction is possible, provided both the (000$\bar{1}$)Se and (000$\bar{1}$)Cd surfaces are simultaneously high in energy, relative to all other surfaces, e.g., due to a reduced tendency of surfactants to bind to these surfaces. This, in fact, has been observed in the case of surfactant ligands such as tetradecylphosphonic acid and hexylphosphonic acid, in which cases growth along the (000$\bar{1}$) direction is believed to occur.[1]

Finally, we note that *symmetric* anisotropic growth (i.e., comparable growth rates along both (0001) and (000$\bar{1}$) directions) is highly improbable in wurtzite CdSe systems owing to the requirement of high surface energies of all four polar surfaces, which is difficult to achieve given the vastly different magnitudes of the four surface energies and their chemical potential dependences. It is reasonable to assume that such symmetric growth is also improbable in other wurtzite systems, providing a rationale for the diversity of nanostructure shapes that have been successfully created in the past.

VI. Summary

We have presented a comprehensive ab initio study of clean and oxygen-covered polar and nonpolar wurtzite CdSe surfaces. The ordering and relative magnitudes of the surface energies are used to comment about the possibility of asymmetric and anisotropic growth in these systems. Our results can be summarized as follows:

(a) Among the clean surfaces, the nonpolar ones (containing equal numbers of Cd and Se atoms at the surface plane) display the most relaxation, while the polar ones (which are either Cd- or Se-terminated) show almost no tendency for relaxation. This

behavior is consistent with the formal electron counting and redistribution rules for II−VI semiconductor systems.

(b) On nonpolar facets, oxygen adsorption selectively takes place on surface Se atoms (driven by an accumulation of electrons at these sites), resulting in a significant decrease in the surface energy of these facets from their clean surface values. This renders all the nonpolar facets passive toward further growth in the presence of oxygen.

(c) Study of oxygen adsorption on polar facets for a range of oxygen coverage and on three different adsorption sites (on-top, bridge, and 3-fold) revealed that, for appropriate choices of the Cd chemical potential and oxygen coverage, the surface energies of the two (0001) facets (one of which is Cd-terminated and the other is Se-terminated) are far higher than those of the other surfaces. On the other hand, among the two (000$\bar{1}$) surfaces, the Se-terminated facet displays low surface energy regardless of the choice of the Cd chemical potential, although the Cd-terminated facet has high surface energy under Cd-poor conditions. Since growth along one of the polar axes involves interconvertible creation of both Cd- and Se-terminated facets along that direction (which requires high surface energies for both interconvertible facets), the above results imply that growth along the (0001) direction will be favored over the (000$\bar{1}$) direction, in the presence of oxygen.

(d) Finally, the approach presented in this paper to quantify the degree of asymmetric anisotropic growth relies on the computation of surface energies as a function of precursor concentration (e.g., Cd chemical potential) and surfactant concentration (e.g., oxygen coverage). This approach is very general, and has the potential to provide guidance for the creation of novel shapes through control of the relative magnitude and ordering of the surface energies, and hence growth directions, by identifying the appropriate chemical environment.

References and Notes

(1) Manna, L.; Scher, E. C.; Alivisatos, A. P. *J. Cluster Sci.* **2002**, *13* (4), 521–532.

(2) Murray, C. B.; Norris, D. J.; Bawendi, M. G. *J. Am. Chem. Soc.* **1993**, *115*, 8706–8715.

(3) Manna, L.; Scher, E. C.; Alivisatos, A. P. *J. Am. Chem. Soc.* **2000**, *122*, 12700–12706.

(4) Nozik, A. *J. Inorg. Chem.* **2005**, *44*, 6893–6899.

(5) Huynh, W. U.; Dittmer, J. J.; Alivisatos, A. P. *Science* **2002**, *295*, 2425.

(6) Colvin, V. L.; Schlamp, M. C.; Alivisatos, A. P. *Nature* **1994**, *370*, 354–357.

(7) Chan, W. C. W.; Nie, S. *Science* **1998**, *281*, 2016–2018.

(8) Jaiswal, J. K.; Mattoussi, H.; Mauro, J. M.; Simon, S. M. *Nat. Biotechnol.* **2002**, *21*, 47–51.

(9) Klimov, V. I.; Mikhailovsky, A. A.; Xu, S.; Malko, A.; Hollingsworth, J. A.; Leatherdale, C. A.; Eisler, H. J.; Bawendi, M. G. *Science* **2000**, *290*, 314–317.

(10) Bodineau, T.; Ioffe, D.; Velenik, Y. *J. Math. Phys.* **2000**, *41*, 1033–1098.

(11) Talapin, D. V.; Koeppe, R.; Go1tzinger, S.; Kornowski, A.; Lupton, J. M.; Rogach, A. L.; Benson, O.; Feldmann, J.; Weller, H. *Nano Lett.* **2003**, *3*, 1677–1681.

(12) Yu, W. W.; Wang, Y. A.; Peng, X. *Chem. Mater.* **2003**, *15*, 4300–4308.

(13) Wang, L. G.; Pennycook, S. J.; Pantelides, S. T. *Phys. Rev. Lett.* **2002**, *89*, 075506(1)–075506(4).

(14) Manna, L.; Wang, L. W.; Cingolani, R.; Alivisatos, A. P. *J. Phys. Chem. B* **2005**, *109* (13), 6183–6192.

(15) Rempel, J. Y.; Trout, B. L.; Bawendi, M. G.; Jensen, K. F. *J. Phys. Chem. B* **2006**, *110* (36), 18007–18016.

(16) Wang, Q.; Pan, D.; Jiang, S.; Ji, X.; An, L.; Jiang, B. *J. Cryst. Growth* **2006**, *286*, 83–90.

(17) Shieh, F.; Saunders, A. E.; Korge, B. A. *J. Phys. Chem. B* **2005**, *109* (18), 8538–8542.

(18) Andelman, T.; Gong, Y.; Polking, M.; Yin, M.; Kuskovsky, I.; Neumark, G.; O'Brien, S. *J. Phys. Chem. B* **2005**, *109*, 14314–14318.

(19) Cheng, Y.; Wang, Y.; Bao, F.; Chen, D. *J. Phys. Chem. B* **2006**, *110*, 9448–9451.

(20) Chen, F.; Zhou, R.; Yang, L.; Liu, N.; Wang, M.; Chen, H. *J. Phys. Chem. C* **2008**, *112*, 1001–1007.

(21) Lee, S. M.; Cho, S. N.; Cheon, J. *Adv. Mater.* **2003**, *15* (5), 441–444.

(22) Wang, Z. L.; Kong, X. Y.; Zuo, J. M. *Phys. Rev. Lett.* **2003**, *91*, 185502(1)–185502(4).

(23) Ma, C.; Ding, Y.; Moore, D.; Wang, X. D.; Wang, Z. L. *J. Am. Chem. Soc.* **2004**, *126*, 708–709.

(24) Wang, Y.; Wang, G. Z.; Yau, M. Y.; To, C. Y.; Ng, D. H. L. *Chem. Phys. Lett.* **2005**, *407*, 510–515.

(25) Peng, X. G.; Manna, L.; Yang, W. D.; Wickham, J.; Scher, E.; Kadavanich, A.; Alivisatos, A. P. *Nature* **2000**, *404*, 59–61.

(26) Li, R.; Lee, J.; Yang, B.; Horspool, D.; Aindow, M.; Papadimitrakopoulos, F. *J. Am. Chem. Soc.* **2005**, *127*, 2524–2532.

(27) Ding, Y.; Ma, C.; Wang, Z. L. *Adv. Mater.* **2004**, *16*, 1740–1743.

(28) Li, R.; Luo, Z.; Papadimitrakopoulos, F. *J. Am. Chem. Soc.* **2006**, *128*, 6280–6281.

(29) Rempel, J. Y.; Trout, B. L.; Bawendi, M. G.; Jensen, K. F. *J. Phys. Chem. B* **2005**, *109*, 19320–19328.

(30) Puzder, A.; Williamson, A. J.; Zaitseva, N.; Galli, G.; Manna, L.; Alivisatos, A. P. *Nano Lett.* **2004**, *4*, 2361–2365.

(31) Soler, J. M.; Artacho, E.; Gale, J. D.; Garcia, A.; Junquera, J.; Ordejon, P.; Sanchez-Portal, D. *J. Phys.: Condens. Matter* **2002**, *14*, 2745–2779.

(32) Martin, R. *Electronic Structure: Basic Theory and Practical Methods*; Cambridge University Press: New York, 2004.

(33) Troullier, N.; Martins, J. L. *Phys. Rev. B* **1991**, *43*, 1993–2006.

(34) Sadowski, T.; Ramprasad, R. *Phys. Rev. B* **2007**, *76*, 235310(1)–235310(5).

(35) Yu, M.; Fernando, G. W.; Li, R.; Papadimitrakopoulos, F.; Shi, N.; Ramprasad, R. *Appl. Phys. Lett.* **2006**, *88*, 231910(1)–231910(3).

(36) *CRC Handbook of Chemistry and Physics*, 76th ed.; CRC Press: New York, 1996.

(37) Zhang, S. B.; Wei, S. H. *Phys. Rev. Lett.* **2004**, *92*, 086102(1)–086102(4).

(38) Peng, Z. A.; Peng, X. *J. Am. Chem. Soc.* **2002**, *124*, 3343–3353.

(39) Getman, R. B.; Xu, Y.; Schneider, W. F. *J. Phys. Chem. C* **2008**, *122*, 9559–9572.

(40) Srivastava, G. P. *Rep. Prog. Phys.* **1997**, *60*, 561–613.

(41) Pashley, M. D. *Phys. Rev. B* **1989**, *40*, 10481–10487.